



A microcalorimetric study of methane adsorption on activated carbons obtained from mangosteen peel at different conditions

Liliana Giraldo¹ · Paola Rodriguez-Estupiñan² · Juan Carlos Moreno-Piraján²

Received: 22 April 2017 / Accepted: 5 January 2018 / Published online: 17 January 2018
© Akadémiai Kiadó, Budapest, Hungary 2018

Abstract

Mangosteen peel was used as precursor for four series of activated carbons (ACs) for methane adsorption obtained by chemical activation. The activating agent-to-char ratios (AA/char) using H_3PO_4 , $ZnCl_2$, K_2CO_3 and KOH and the temperature were studied, to correlate these parameters with the methane adsorption capacity. The results showed that $ZnCl_2$ —AC—have a higher methane adsorption capacity ($178 \text{ cm}^3 \text{ cm}^{-3}$) compared to the other activated carbons, which presented a good methane adsorption capacity. Methane adsorption was monitored by adsorption microcalorimetry, and higher enthalpic values were found for the smaller micropores.

Keywords Adsorption calorimetry · Mangosteen peel · Activated carbons · Methane storage

Introduction

Petroleum, its by-products and its uncontrolled use have created a critical and increasing greenhouse effect on the planet. Because of this, it is necessary to seek new sources of clean energy. For several decades, natural gas has become a possible alternative to conventional fuels due to its low price, and it is the fossil energy that pollutes the least, because of its complete combustion and lower production of gaseous and solid pollutants [1], and also it has the highest energy efficiency. Three methodologies for natural gas storage are known: (1) liquefied natural gas (LNG), (2) compressed natural gas (CNG) and (3) adsorbed natural gas (ANG). Some disadvantages have been

associated with these methodologies. In the case of LNG, the high cost of liquefaction, the requirement of special insulated containers and the potential fire hazard hinder its upscaling. The CNG is the most commercialized form of natural gas, but the high operating pressure (200–250 bar) is once again a difficulty in its handling and availability for specific uses [1–4].

ANG has been an active field of study in the last years; in this methodology, natural gas is stored in adsorbent materials (porous solids) as the adsorbed phase. Natural gas adsorption of porous solids has the advantage of operating at low pressure and at room temperature, constituting a safe and low-cost way to store methane for natural gas vehicles and comparable to other conventional petroleum-based fuels. Nowadays one of the main goals in the ANG application is the preparation of adsorbents with adequate characteristics and the development of technics that allow studying the adsorption process [5–9]. For proper natural gas storage using the ANG system, it is necessary to prepare porous materials whose microporosity and surface area are large for a high capacity of methane storage [10–12].

In scientific literature, some articles have reported the preparation of porous solids with appropriate storage characteristics for methane. Materials commonly used to prepare activated carbon are agricultural wastes, coal, among others [12–14]. Recently, other materials such as

✉ Juan Carlos Moreno-Piraján
jumoreno@uniandes.edu.co

Liliana Giraldo
lgiraldogu@unal.edu

Paola Rodriguez-Estupiñan
jp.rodriguez@uniandes.edu.co

¹ Facultad de Ciencias, Departamento de Química, Universidad Nacional de Colombia, Carrera 30 # 45-03, Bogotá, Colombia

² Facultad de Ciencias, Departamento de Química, Grupo de Investigación en Sólidos Porosos y Calorimetría, Universidad de los Andes, Carrera 1 #18A-12, Bogotá, Colombia

MOFs, aerogels, xerogels and others have been explored for methane storage [12–16]. Different methane adsorption capacities expressed in volume (V/V) have been reported ranging from 146 to 240 (cm³(STP) cm⁻³) using different pressures [1–16].

The use of the agricultural residues for the preparation of activated carbon and its application in different areas is an interesting, since it contributes to the reduction in the environmental impact generated by these residues. The mangosteen is a tropical fruit (*Garcinia mangostana* L.) known as the “queen of fruits” among other reasons for its medical properties. India, Thailand and Vietnam are the world’s largest producers. In Colombia (South America), this fruit has reached high production levels, but its consumption generates wastes (peel), which gradually ferment and release odors that can potentially affect the public health [17–19]. According to the information above, it is proposed to use mangosteen peel (MP) to produce activated carbon (AC) and exploring their potential for methane storage. This can increase the added value of these wastes and can reduce the cost of final disposal [18, 19].

In this work, activated carbons were prepared from mangosteen peel (MP) by chemical activation with different chemicals like activating agents; the effect of the temperature on methane storage capacity was also analyzed. In addition, the adsorption process is monitored by adsorption microcalorimetry to investigate the role of pore size and was correlated with other properties established by conventional methods.

Experimental

Raw materials

Mangosteen peel (MP) used for the preparation of activated carbons was collected in a marketplace in Bogotá (Cundinamarca, Colombia). MP was washed with distilled water to remove sludge and other impurities from their surface. The treatment used to process the samples was reported in the literature with some variations [17–20]. Subsequently, the samples were dried at 105 °C for 48 h to remove the moisture content. The chemical reagents used in this research were of analytical grade.

A proximate and ultimate analysis was carried out on MP. For the proximate analysis, ASTM standards were used [21], while an elemental analyzer (Carlo Erba, model EA-1108) was used for the ultimate analysis (C, H, N and O).

The results are summarized in Table 1 and show that the mangosteen peels have a fixed carbon content and low ash content, which makes it a suitable material as a precursor for activated carbon.

Table 1 Proximate and ultimate analysis of mangosteen peel (on dry basis)

Proximate analysis	Mass%	Ultimate analysis (dry basis)	Mass%
Moisture	3.6	Carbon	49.34
Volatile matter	66.2	Oxygen	42.32
Ash	2.3	Hydrogen	5.12
Fixed carbon	27.9	Nitrogen	1.24

Preparation of activated carbons

Activated carbon samples were prepared with the pre-treated mangosteen peel (MP) described above. The detailed procedure was as follows: 70 g of MP was put in a quartz cell in such a way that the nitrogen was in contact with the whole MP sample. The quartz cell was placed inside a quartz tube, and both were placed into a CarboliteTM furnace model CTF 12/TZF 12.

The MP was carbonized at 450 °C with a heating rate of 10 °C min⁻¹ for 3 h. (Time was not modified throughout this investigation.) Then, chars were treated with a 40% (w/v) solution of the respective chemical activating agents: H₃PO₄, ZnCl₂, K₂CO₃ and KOH. To obtain each sample at each impregnation ratio, 50 g of MP char was placed in a beaker and impregnated at 60 °C for 180 min, ensuring that the whole mass was wetted with the respective activating agent/char ratio (0.5–2.0). Afterward, the solid was separated and prepared for the thermal process.

The solids were activated for 180 min at different temperatures (700, 800 and 900 °C) with a heating ramp 10 °C min⁻¹ and a nitrogen flow of 150 mL min⁻¹ (99.999% purity). Activated carbons were designated as follows: MPP, MPZ, MPC and MPK, for activated carbon with H₃PO₄, ZnCl₂, K₂CO₃ and KOH, respectively. Table 2 relates the nomenclature with the preparation conditions. For example, MPP4 corresponds to a solid impregnated with H₃PO₄ solution at an activating agent/char ratio of 2.0 at 800 °C. The temperatures of the carbonizations and activations of the solids were chosen according to previous results with similar lignocellulosic materials [22–25].

Once the activated carbons were obtained, they were washed according to the activating agent employed:

- Those activated with H₃PO₄: were washed with hot water several times until the filtrate had a constant pH.
- The ZnCl₂-activated samples were washed in a Soxhlet extractor using 300 mL of 3 M HCl solution for 1 h, followed by washing with deionized water until no chloride ions were detected.

Table 2 Activation parameters and yield% and properties of the samples

Sample	Adsorbed characteristics				
	AA/char ratio/w/w	Temperature/°C	Time/min	Yield/% ^a	<i>I</i> ₂ (IN)/mg g ⁻¹
MPP1	0.5	800	180	32.4	960
MPP2	1.0	800	180	31.1	1050
MPP3	1.5	800	180	30.6	1267
MPP4	2.0	800	180	29.5	1187
MPZ5	0.5	800	180	34.5	1045
MPZ6	1.0	800	180	43.5	1240
MPZ7	1.5	800	180	40.0	1560
MPZ8	2.0	800	180	37.4	1330
MPC9	0.5	800	180	22.4	865
MPC10	1.0	800	180	21.2	970
MPC11	1.5	800	180	20.0	1050
MPC12	2.0	800	180	18.7	966
MPK13	0.5	800	180	25.5	932
MPK14	1.0	800	180	24.8	1021
MPK15	1.5	800	180	23.7	1237
MPK16	2.0	800	180	22.6	1142
MPP17	1.5	700	180	31.4	1100
MPP18	1.5	900	180	30.3	1250
MPZ19	1.5	700	180	38.9	1450
MPZ20	1.5	900	180	37.4	1585
MPC21	1.5	700	180	21.5	1020
MPC22	1.5	900	180	20.4	1100
MPK23	1.5	700	180	24.9	1265
MPK24	1.5	900	180	22.1	1187

The yield (%) of carbonization process is calculated according to the following formula; Yield (%) = $\left(\frac{W_{\text{after}}}{W_{\text{before}}}\right) \times 100$ where W_{before} is mass of mangosteen peel, W_{after} is mass of carbon product from carbonization

^aMPP, MPZ, MPC and MPK, for activated carbon with H₃PO₄, ZnCl₂, K₂CO₃ and KOH, respectively

- (c) The samples activated with K₂CO₃: were washed with 0.1 M HCl solution to dissolve ash and inorganic salts. Finally, deionized water was used to wash samples of this activated carbon until constant pH in the filtrate water.
- (d) Samples activated with KOH: after activation the sample was washed with deionized water several times and then treated with hydrochloric acid (100 mL HCl and 300 mL deionized water) to remove excess activating agent and inorganic matter residues from the sample and then washed again with deionized water until constant pH.

the starting material was evaluated by TGA–DTA between 30 and 900 °C with a heating rate of 10 °C min⁻¹. A thermogravimetric analyzer (Hitachi TGA/SDTA Model 7200) was used. It was measured under an atmosphere of N₂ with a flow rate of 100 cm³ min⁻¹.

Iodine number determination

Iodine number is a widely used technique to determine the adsorption capacity of porous solid. It is defined as the milligrams of iodine adsorbed by 1.0 g of carbon, often reported in mg g⁻¹ with a typical range between 500 and 1200 mg g⁻¹. Iodine number is a measure of the equilibrium mass of iodine adsorbed on a surface from excess. It is a standard test method. The iodine adsorption was determined using the sodium thiosulfate volumetric method [26–28].

Iodine number can be associated with the porosity of activated carbon, and it is a measure of activation level, so

Characterization of activated carbons

TGA–DTA

The TGA was also used to determine the maximum rate of mass loss of organic compounds. The thermal behavior of

a higher number indicates higher degree of activation. Consequently, the iodine number can be related to micropore content of the activated carbon by adsorption of iodine from solution [26–28].

N₂ isotherms at – 196 °C

The porous structure of the activated carbons prepared in this work was determined by the nitrogen adsorption–desorption isotherms at – 196 °C using an IQ2 sorptometer (Quantachrome Instruments, Miami, FL, USA) and its software to calculate the textural characteristics: BET area and pore size distribution by density functional theory (i.e., NLDFT and QSDFT) [29, 30]. Prior to measurements, the activated carbon samples were degassed at 250 °C in an inert atmosphere for 24 h to remove moisture or contaminants pre-adsorbed on the activated carbons [31].

The nitrogen adsorption isotherms were obtained on a relative pressure P/P° for a pressure range between $10^{-6} < P/P^\circ < 0.99$ [32, 33]. The specific surface areas of the activated carbons were estimated by the Brunauer–Emmett–Teller model (BET) by the multipoint nitrogen adsorption method in the range of $0.05 < P/P^\circ < 0.3$ [31–34]. The microporous surfaces (S_{mic}) as well as the total volumes (V_{tot}) and micropores volumes (V_{mic}) were evaluated by the t-plot method [35]. The width pore, D_p , was calculated from the density functional theory (DFT) applied to the nitrogen adsorption isotherm using the Quantachrome Inc. software. The pore size distributions (PSDs) were calculated by applying the Quenched Solid Density Functional Theory, equilibrium model (QSDFT) [29, 30, 32, 33].

Methane adsorption isotherm measurements at high pressure

The methane adsorption experiments were carried out at 25 °C and up to a pressure of 5 MPa in high-pressure adsorption automatic equipment (HPVA II, Micromeritics). All samples were heated at 250 °C under vacuum for 3 h to remove water adsorbed and other contaminants before methane adsorption measurements. The cold volume measurement was taken at 20 °C and then changed to 25 °C for the hot volume measurement and for the adsorption experiments. The pressure range for the adsorption was 0.15–5 MPa. The pressure for desorption was 10^{-2} MPa. The contribution of the empty cell was systematically measured and subtracted to all data in order to improve accuracy. The amount of material within the sample cell was about 1.000 g. Calibration of the empty space using helium and the methane isotherms was performed according to procedures presented in the literature [36, 37].

Methane differential enthalpy measurement by adsorption calorimetry

The differential enthalpy of methane adsorption measurements on the activated carbon samples was obtained in a high-sensitivity Tian–Calvet heat-flow microcalorimeter, suitable for the study of the gas–solid interactions. This equipment, which has been described in the literature [38, 39], was designed and built in porous solids and calorimetry laboratory (Author’s Laboratory). This instrument is not only less expensive than a commercial system, but it is also easier to be operated.

The microcalorimeter uses two calorimetric cells: The first one contains the sample, and the second one, through which the gas or vapor, methane in this case, passes is the reference; therefore, it is usually empty. The cells are designed and built in stainless steel to withstand working pressures and to avoid physical or chemical interactions with the adsorbate. As mentioned above, the calorimeter used in this research (Tian–Calvet, in honor of its creators Albert Tian and Edouard Calvet of the Faculty of Sciences of Marseille—France) corresponds to a passive-type diathermal calorimeter because the energy exchange is performed by heat conduction. With this type of calorimetry, only the energy effect of the system being studied is recorded because the reference cell eliminates the foreign processes related to the undesired interactions: for example diffusion of gases among others.

The adsorption pressures in the measurements were monitored with Baratron pressure transducers to record low pressures and Honeywell-type Model HP High Pressure Transducer to record the changes at high pressures. Prior to each experiment, the samples were degassed at 250 °C and 1×10^{-6} MPa. Once the temperature was reached, it was held for 24 h. The use of these temperatures allows to eliminate the impurities adhered to the prepared carbon materials, and their properties are not altered due to the stability and nature of the material. Subsequently, it was cooled to room temperature at the same rate.

The calorimeter was calibrated electrically in order to establish its correct operation as well as to convert the voltage–time signal into units of energy. The procedure followed was reported in the scientific literature [38, 39]. A brief summary of this procedure is: An Agilent™ voltage source (model E3649A) dissipated electrical work through a 640-kΩ ceramic resistor. Subsequently, the electrical potential generated by an Agilent 34401™ 6½-digit multimeter was recorded, in order to simulate the thermal effects generated in each addition of adsorbate. Different levels of electrical work were dissipated to establish the repeatability of the calorimeter constant. The constant

established for this equipment after 10 determinations was $25.4 \pm 0.3 \text{ WV}^{-1}$.

The experiments were conducted in an isothermal manner by gradually feeding increasing doses of methane over previously degassed samples. The initial dose sent to the system corresponded to a pressure of 10 mbar. Since the initial dose was sufficiently small, the heat obtained can be considered as a differential adsorption heat. A new dose of methane (10 mbar) was then added, until equilibrium pressure was achieved. Subsequently, the methane dose was increased, and the procedure was repeated until no change in pressure was observed. This was achieved at around 50 bar (5 MPa).

The calorimeter allows sensing the heat generated by each dose added, and the pressure drop in the cell allows obtaining the amount adsorbed. For each dose, the thermal equilibrium was reached before the first dose, P_i (initial pressure); the adsorbed amounts δn_{ads} and the integral heats generated were measured. The calorimetric adsorption experiments finished when the released heat at a relatively high pressure and the increase in adsorbed amount were insignificant [31–33, 38, 39].

The adsorption differential heat was obtained from the data obtained by microcalorimetry; the enthalpy was calculated by dividing the heat by the moles amount adsorbed for each dose. The adsorption heats were determined by the integration of the calorimetric data and the amount of adsorbed molecules which were evaluated using each pressure value. The adsorbed amounts were expressed as mmol g^{-1} by samples degassed at $250 \text{ }^\circ\text{C}$. The calorimetric data were reported here as differential enthalpy, $\Delta H_{\text{diff}} = \delta Q_{\text{int}}/\delta n_{\text{ads}}$. The results can also be reported as integral adsorption enthalpy, ΔH_{int} [31–35]. The results can be presented as ΔH_{diff} versus adsorbed amount of methane, ΔH_{diff} versus pore size or ΔH_{diff} versus pressure.

Results and discussion

Effect of temperature and the activating agent/char ratio (AA/char) of MP on the textural properties

In the preparation of activated carbons for specific applications, it is necessary to take into account the yield, BET surface, pore volume among other characteristics. In this work, two widely known factors that influence the activation of biomass [20, 40] were investigated: activating agent/MP char ratio and temperature. The activation time was fixed at 3 h (180 min), according to literature reports for lignocellulosic materials [20, 41, 42] and in this way establishes the influence of these two variables on the textural properties, methane adsorption capacity and

differential enthalpies of adsorption of the activated carbon obtained from MP. The relationship between iodine number (IN) and the internal surface area in terms of $\text{m}^2 \text{g}^{-1}$ for various precursors has been widely reported [20].

The results presented in Table 2 correspond to the four series of activated carbons prepared in this work: MPP, MPZ, MPC, MPK (H_3PO_4 , ZnCl_2 , K_2CO_3 and KOH , respectively) which show that IN increases as a function of the AA/char ratio, and thus, $\text{MPZ} > \text{MPP} > \text{MPK} > \text{MPC}$. If S_{BET} is plotted in function of IN, a linear correlation could be found (see Fig. 1), which can be described by the following equation:

$$y = 1.0854x + 10.203R^2 = 0.8865$$

or can be expressed as:

$$S_{\text{BET}} = 1.0854\text{IN} + 10.203$$

The effect of the AA/char ratio on the textural properties of each AC increased with increasing the ratio to 1.5 and then a decrease occurred. This may be associated with AA/char ratio, an excess of the activating agent, as well as small traces of metals and/or salts (produced during the activation) could be blocked. In addition, this behavior could be attributed to this: During the carbonization process of lignocellulosic materials like mangosteen peel, the C, O and H atoms can react to form CO , CO_2 , H_2O , CH_4 , aldehydes or tar, as it has been mentioned by some authors [43]. Therefore, the yield will depend on the amount of carbon released and its combination with O and H atoms.

For example, when using ZnCl_2 as activating agent, the activated MP with lower ratio of ZnCl_2 had the lowest yield (34.5%); this is due to the amount of carbon removed as CO , CO_2 , CH_4 and tar. However, ZnCl_2 can selectively separate H and O from MP as H_2O and H_2 instead of CO , CO_2 or hydrocarbons [43] so the yield was higher (40%). Finally, with increasing ratio of AA/char (2.0) there was a greater carbon release and the micropore size slightly

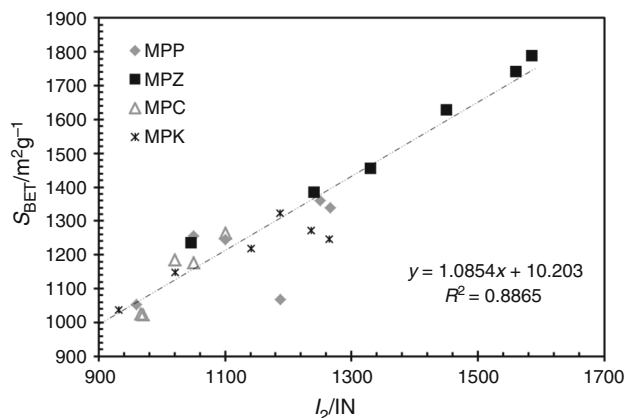


Fig. 1 Relation between IN and S_{BET}

changed to mesopores with extra ZnCl_2 , resulting in a lower yield compared to the series.

On the other hand, the study was carried out at different activation temperatures (700 and 900 °C) with a fixed AA/char ratio (1.50) and at a fixed time (180 min). The results showed that at higher temperatures the activated carbon got some higher textural properties like BET surface area, total pore volume, micropore volume and width pore. The result indicated that at a higher temperature the reaction rate between char and the respective activating agent led to the release of more volatile compounds generating more surface area and porosity. A decrease in the yield at higher temperatures that can be associated with the improvement in the textural characteristics was observed [20]. A higher temperature provides a better condition for activated carbon preparation and higher adsorption properties. The results of the present work are in good agreement with other studies with similar materials [20, 44].

TGA analysis of mangosteen peel

Thermogravimetry is used to understand the thermal behavior of different materials including biomass. The thermogravimetric analysis (TGA) profile of the raw material clearly showed an approximation about the mass loss with respect to temperature due to the release of moisture and volatile matter. Figure 2 shows the mangosteen peel (MP) TGA–DTA curve. Mangosteen is classified as a lignocellulosic material composed mainly of lignin, cellulose and hemicellulose, which usually add up to about 70%. The decomposition reactions for this type of material have been widely described in the literature [20, 45, 46]:

Biomass \rightarrow solid residue + volatile

The mangosteen peel decomposition occurred in four stages as has been reported in the literature [20, 46]. There was an initial mass loss starting at 80 °C until 120 °C; the slope change was associated with a process of desorption of free and anchored water to the matrix of the mangosteen peel. The second stage in the TGA profile describes a

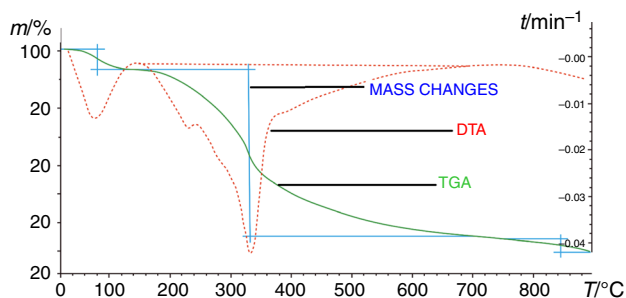


Fig. 2 Thermogravimetric–differential thermogravimetric curve of raw mangosteen peel

strong loss of mass because of the rapid decomposition of cellulose and hemicellulose to volatiles materials and tars; it was between 200 and 340 °C [20, 45]. Subsequently, a mass loss was observed in the temperature range of 340–700 °C and then a low rate of mass loss at temperatures above 520 °C. The mass loss above 340 °C has been attributed mainly to the carbonization process of lignin and possibly cracking of C–C bonds. Thermograms confirmed the chosen carbonization temperature to obtain the char of mangosteen peel [20, 46–48]. Some authors have suggested [30, 32] that lignin gradually decomposes to 740 °C and at the same time the residual volatiles of the first stage are released and the fixed carbon remains. However, after 700 °C, the thermal decomposition of the mangosteen peel was practically complete, and this was another reason to choose the temperature to carry out the activations of the biomass (700, 800 and 900 °C).

Above 800 °C, the mass loss was small, because of the reorganization of the carbon matrix and an increase in the polyaromatic carbon [46].

In summary, pyrolysis of biomass contains three main stages over whole temperature range, which was: moisture drying, major degradation of the more unstable polymers and consecutive minor devolatilisation. Undoubtedly, these last two steps are relevant with the chemical composition and bonding of the lignocellulosic structure since main constituents of the biomass have different degradation behaviors. The pyrolysis of biomass normally can be explained by three main components: cellulose, hemicellulose and lignin [49, 50]. Also, inorganic matter affects the degradation behavior and it has some catalytic effects on biomass pyrolysis. There are no temperature ranges stated for decomposition of lignin, cellulose and hemicellulose, but it is believed that lignocellulosic biomass is stable until 200 °C. At lower temperatures, minor mass losses occur due to removal of moisture and the hydrolysis of compounds [50]. Hemicellulose and cellulose decomposition are believed to have occurred in the temperature ranges of 200–350 and 200–500 °C, respectively [51]. The decomposition rate of lignin is quite slower than hemicellulose and cellulose in a wider temperature range of 150–900 °C [52–56].

Activated carbons characterization

The N_2 adsorption–desorption isotherms and the pore size distributions of the activated carbons prepared from MP under different conditions presented a narrow knee at low relative pressures, suggesting the presence of micropores (see Fig. 3).

All isotherms are type I (b) according to the last classification of the IUPAC [56]. These isotherms are typical of microporous materials with wide pore size distributions

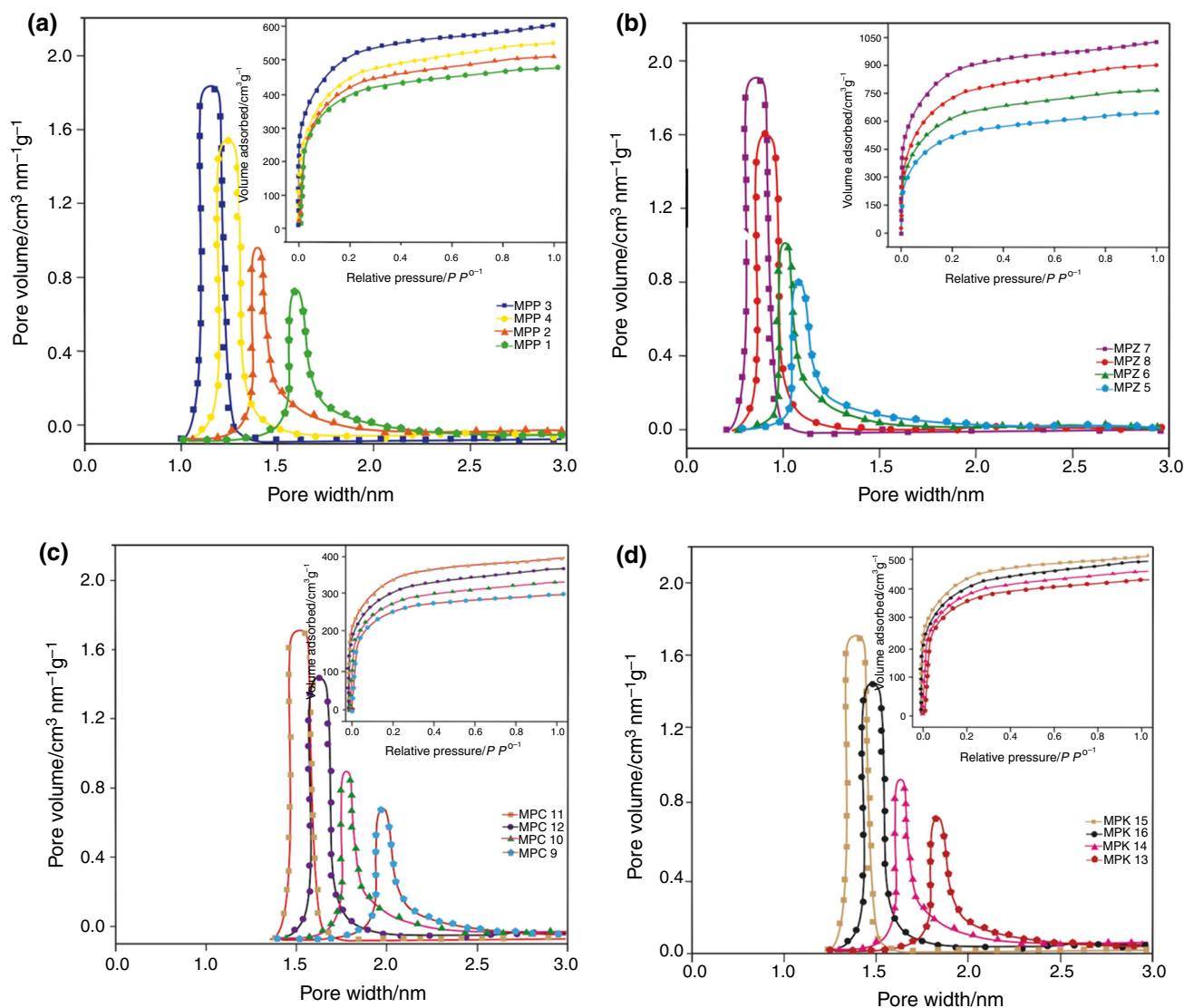


Fig. 3 Pore size distribution and nitrogen adsorption/desorption isotherms (inset). **a** Varying AA/char for MPP, **b** varying AA/char for MPZ, **c** varying AA/char for MPC, **d** varying AA/char for MPK (preparation conditions: activation temperature: 800 °C and activating time 180 min)

including narrow and wider ($< \sim 2.5$ nm) micropores [56]. For all samples, it could be observed (see Fig. 2a–e) that in the initial part a high nitrogen adsorption was followed by a concavity until a limit value (plateau) was reached. This was associated with the pore volume developed in each material, in particular the micropore volume. None of the 24 samples prepared in this work developed cycles of hysteresis from which it was inferred that no mesoporosity was generated with the treatments used.

A detailed analysis of the N_2 isotherms at -196 °C of the activated carbons obtained at different AA/char ratio (0.5–2.0) and activated at 800 °C and 180 min shows that at AA/char ratio = 1.5 the activated carbons presented greater capacity of adsorption (see Fig. 3a–d).

On the other hand, the N_2 adsorption isotherms of the activated carbons prepared at different temperatures (not

shown here) with AA/char ratio = 1.5 and activation time of 180 min show that for all activated samples prepared at 900 °C nitrogen amount adsorbed were greater than those that are activated at 700 °C.

Table 3 shows the S_{BET} , S_{mic} , the ratio between these two variables, pore volumes (total, and micropores), ratio between these volumes and width pore of the activated carbons prepared. The results indicated that among four activating agents used to obtain activated carbons from MP, the $ZnCl_2$ was the one that produced activated carbons with the best textural characteristics.

Studies based on the AA/char ratio show that textural variables (S_{BET} , S_{mic} , $S_{mic}/S_{BET}(\%)$, V_{tot} ($cm^3 g^{-1}$), V_{mic} ($cm^3 g^{-1}$), V_{mic}/V_{tot}) increase as a function of the increase in the AA/char ratio reaching a maximum value in sample ($S_{BET} = 1747 m^2 g^{-1}$) and then decrease in sample MPZ8

Table 3 Effect of activation temperature and impregnation ratio on BET surface areas, pore volumes, average pore sizes of activated carbons by H_3PO_4 , $ZnCl_2$, KOH and K_2CO_3

Sample	$S_{BET}/m^2 g^{-1}$	$S_{mic}/m^2 g^{-1}$	$S_{mic}S_{BET}^{-1}/\%$	$V_{tot}/cm^3 g^{-1}$	$V_{mic}/cm^3 g^{-1d}$	$V_{mic}V_{tot}^{-1}/\%$	D_p/nm
MPP1	1052	976	92.78	0.88	0.76	86.36	1.16
MPP2	1255	1189	94.74	0.95	0.83	87.37	1.20
MPP3	1340	1278	95.37	1.09	0.97	89.00	1.25
MPP4	1067	997	93.44	0.89	0.78	87.64	1.36
MPZ5	1236	1187	96.04	0.94	0.83	88.29	0.81
MPZ6	1387	1356	97.77	1.08	0.97	89.81	0.89
MPZ7	1743	1714	98.33	1.23	1.12	91.05	0.95
MPZ8	1456	1386	95.19	1.05	0.93	88.57	1.26
MPC9	923	786	85.15	0.77	0.62	80.52	0.70
MPC10	1024	903	88.20	0.83	0.70	84.33	0.76
MPC11	1176	1076	91.49	0.91	0.78	85.71	0.84
MPC12	1025	915	89.26	0.83	0.68	81.92	0.96
MPK13	1035	947	91.50	0.81	0.68	83.95	0.76
MPK14	1147	1089	94.94	0.89	0.76	85.39	0.84
MPK15	1270	1215	95.70	0.96	0.83	86.45	0.95
MPK16	1218	1052	86.37	0.87	0.73	83.90	1.12
MPP17	1245	1137	90.60	0.94	0.78	83.00	1.17
MPP18	1360	1265	93.01	1.18	0.96	81.36	1.34
MPZ19	1630	1567	96.13	1.02	0.90	88.24	0.97
MPZ20	1790	1685	94.13	1.34	1.15	85.82	1.22
MPC21	1185	1043	88.02	0.84	0.68	80.95	0.97
MPC22	1265	1158	91.54	1.04	0.81	77.88	1.03
MPK23	1245	1143	91.80	0.89	0.72	81.00	0.98
MPK24	1323	1215	91.84	1.23	0.98	79.67	1.11

S_{BET} : BET-specific surface area, S_{mic} : micropore-specific surface area, V_{tot} : total pore volume, V_{mic} : micropore volume, D_p : the mean pore (average pore diameter: average pore diameter is estimated using DFT method)

($S_{BET} = 1456 m^2 g^{-1}$) in which the AA/char ratio increases from 1.5 to 2.0. The other activating agents had similar behaviors.

In the scientific literature, the effect of AA as a function of the char has been widely explained [57–59] and in particular the effect of excess chemical agents. The increase in AA accelerates the reaction, so the number of pores increases. When an excessive amount of an AA is added, the values of the textural properties decrease; this is due to an additional reaction between the AA and the carbon of the microporous structure already formed. That is, the addition of an excessive amount of AA can destroy the microporous structure and widen the pores.

The pore size distributions (PSD) oscillate around 2 nm (Fig. 3), showing that all AAs generated microporous activated carbons from MPs according to the IUPAC classification [56] (see Table 3). The pore diameter for each series increases as a function of the AA/char ratio for all activating agents. In the temperature-dependent studies where the ratio AA/char and time were kept constant, the values of the textural properties increased too.

From the N_2 adsorption isotherms at $-196^\circ C$, PSD analysis was carried out using both the non-local density (NLDFT) and the most recently developed: Quenched Solid Density Functional Theory (QSDFT) [60, 61] (results are not shown here).

NLDFT describes the adsorption and fluid phase behavior on a molecular level to obtain pore size information in the micro- and mesopores range. This technique has proven to be a reliable method for characterizing the pore size distribution of a great variety of nanoporous materials; however, the analysis of the pore size of carbons with heterogeneous surfaces is not always well described by this model. The main disadvantage of the NLDFT model is that it does not take into account the chemical and geometric heterogeneity of the pore walls; instead, it assumes an unstructured, chemically and geometrically smooth surface [62, 63].

While the QSDFT model allows representing solids with pores of different geometries, it also takes into account the surface roughness in the disordered carbons, which prevents the occurrence of stratification transitions in the

theoretical DFT isotherms and provides a much more realistic description of the experimental isotherm adsorption. After applying the two models to the experimental nitrogen adsorption data of the activated carbons prepared in this work, the pore size distributions were established by applying the kernel to slit, cylindrical and slit-cylindrical pores. The best fit was the QSDFT model and a slit-cylindrical pore geometry [33].

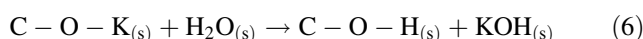
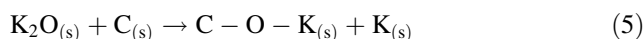
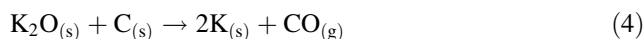
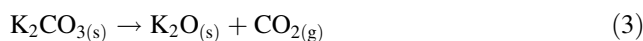
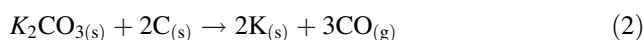
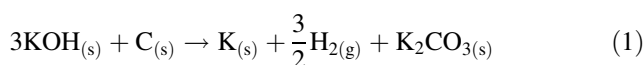
It is worth mentioning that the textural and chemical characteristics that were developed on activated carbons are strongly influenced by the chemical agents used to perform the chemical activation in this work, which were ZnCl_2 , H_3PO_4 , KOH and K_2CO_3 . The effects that have been reported for each of the activating agents will be discussed below:

ZnCl_2 is one of the most widely used chemical agents, but its use has been diminished due to the metal residues and their environmental implications (although it is still used especially in Chinese industries). Initially, the raw material was mixed with the chemical in an aqueous solution to form a paste, which was subsequently evaporated. During evaporation, there was a weakening of the lignocellulosic structure due to hydrolysis reactions (with loss of volatile matter); this leads to an increase in elasticity and a swelling of the precursor. The greater the amount of ZnCl_2 , the stronger the changes would be during impregnation and evaporation. After evaporation, the impregnated carbon was thermally treated in an inert atmosphere at the temperatures reported in this work. ZnCl_2 restricts the formation of tar, avoiding the contraction of the particle and giving rise to a wide and open microporosity (bordering the line between micro- and mesopores). Higher adsorption capacity and higher porosity were obtained in contrast to thermal activation [64].

In the case of the activations with H_3PO_4 when it was mixed with the MP char and it was heating at set temperatures, there was a previous attack on the hemicellulose and the lignin residues. H_3PO_4 could be inserted into the biopolymer chains (hemicellulose, lignin and cellulose), and it could replace the existing bonds in the polymer; then, the glycosidic and aryl ether bond could be hydrolyzed to produce polysaccharides. These reactions lead to a fractionation or reduction in biopolymers; also, they may be accompanied by secondary reactions such as degradation and condensation. During the thermal treatment after the impregnation process there is a continuous production of CO/CO_2 and methane (which does not occur under these temperatures without H_3PO_4). This process also led to reduction in the volume of the particles. When the temperature was increased, the mass loss rate eventually decreased and the structure began to dilate, developing porosity. Apparently, phosphoric acid can combine with organic species to form phosphate bonds, such as

phosphate (metaphosphate) esters and polyphosphate esters attached to biopolymer fragments [64–66].

In the case of activation process of MP char with KOH or K_2CO_3 , the AC obtained was washed with water and HCl solution to remove the soluble salts and to recover the carbon. This step also removed part of the original mineral matter contained in the raw material. KOH is very different from other activating chemicals. The KOH reacts with the carbon skeleton and produces solid and gaseous by-products. The development of porosity of the activated carbons by KOH activation has been associated with gasification reaction. Experimental evidence shows that hydrogen and potassium are commonly formed during the reaction, as well as CO , CO_2 and K_2O . Some authors have proposed the chemical reactions that describe these processes [64, 67, 68]:



In terms of the Gibbs energy, these reactions are thermodynamically possible above 700 °C, and they reflect the experimental evidence evaluated by other authors [67, 68].

The solid potassium compounds formed during the activation diffuse into the carbon matrix internal structure (K intercalation); it acts by widening the existing pores and creating new pores. According to the information above, it is proposed that the increasing the K_2CO_3 or KOH/char ratio improves the activation process and the textural parameters. It was seen a better microporous structure for the activated carbon produced by these activating agents. However, the excess of K_2CO_3 or KOH generates a blockage of the pores and therefore a decrease in the accessible area. This was evidenced for the MCP12 and MPK16 samples. In addition, the pores are widened; there is a decrease in the adsorption capacity and of the carbon yield as well.

In summary, the procedure used in this research allowed obtained samples of activated carbon with different textural characteristics. This is interesting considering the application that will be given in this work: CH_4 storage. With a comprehensive review of the results and reports of the

specialized literature, it was clear that the parameter that must be taken into account to achieve a good storage capacity is the development of micropores (micropore volume) [69].

Methane sorption performance over mangosteen peel-derived AC (MP)

The methane adsorption isotherms at 25 °C to 5 MPa on activated carbons with different AA/char ratios are shown in Fig. 4.

Figure 4a–d shows a rapid increase in the volume of gas adsorbed at low pressures with increasing CH₄ pressure. Then, the increase was lower in medium- and high-pressure ranges.

The CH₄ adsorption capacities were obtained from the starting data: pressure and temperature of the adsorption cell and reference cell, as recommended in the literature [70]: The CH₄ mass was obtained from the cell volume and

vapor density at the pressure and temperature set. The injected CH₄ to the adsorption cell ($m_{\text{adsorption-cell}}$) was divided into two portions: one is partly adsorbed on the solid and the remaining one occupied the void volume of the equipment (V_{void}). Therefore, the adsorbed mass (m_{adsorbed}) is calculated from the following equation:

$$\begin{aligned} m_{\text{adsorbed}} &= m_{\text{adsorbed-cell}} - \rho_{\text{void}} V_{\text{void}} \\ &= m_{\text{adsorption-cell}} - \rho \left(\frac{V_{\text{adsorption-cell}} - m_{\text{ac}}}{\rho_{\text{solid}} - v_{\mu} m_{\text{ac}}} \right) \end{aligned}$$

where ρ_{void} is the CH₄ density as a function of the pressure and temperature of the adsorption cell; $V_{\text{adsorption-cell}}$ is volume of adsorption cell; m_{ac} is the mass of the activated carbon; v_{μ} is the micropore volume of activated carbon. Therefore, the adsorption capacity can initially be calculated as:

$$C = \frac{m_{\text{adsorbed}}}{m_{\text{ac}}}$$

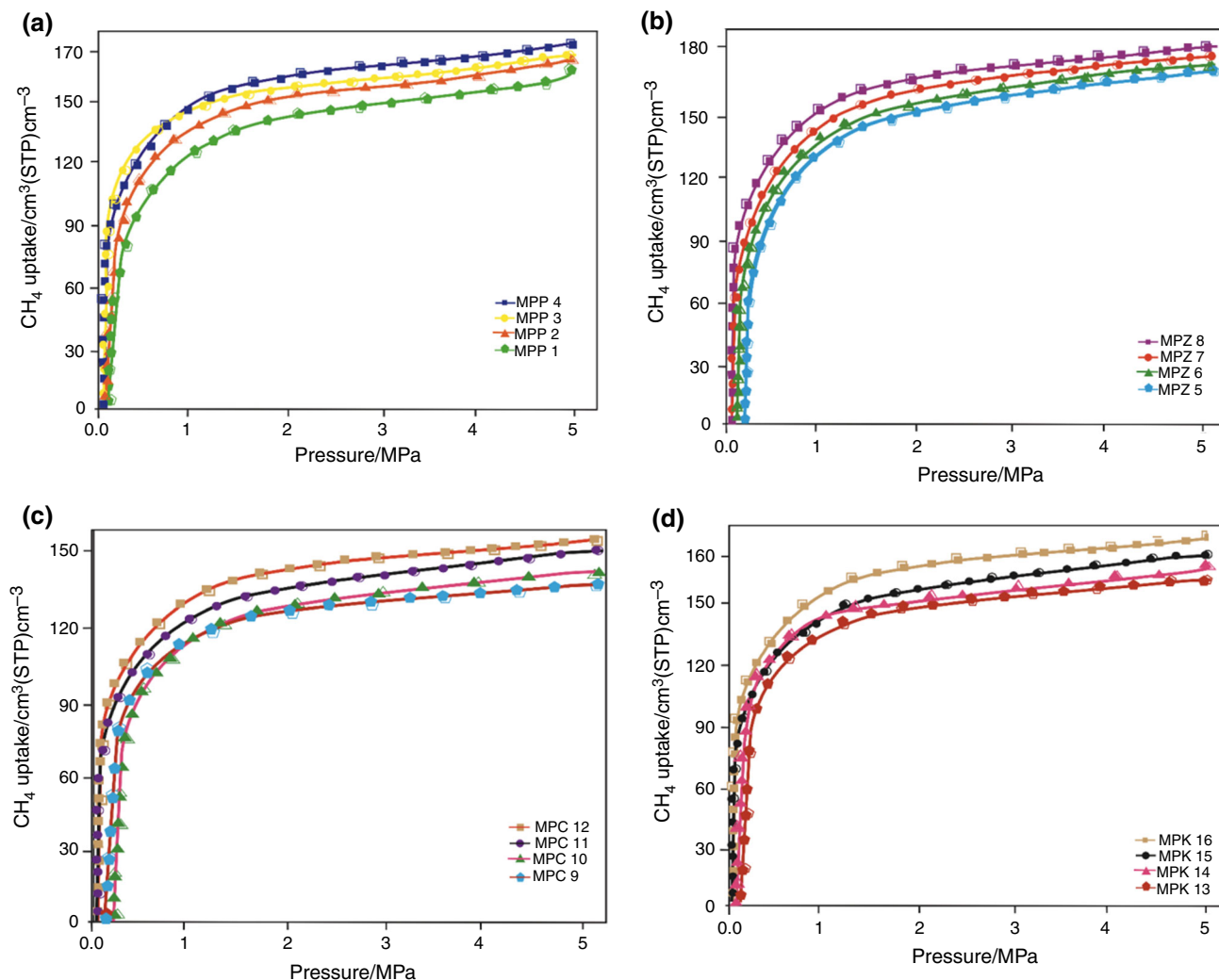


Fig. 4 Methane adsorption isotherms at 25 °C up to 5 MPa for all samples prepared in this research. a MPP, b MPZ, c MPC, d MPK

It can be expressed as wt/wt or V/V [70].

The highest CH₄ adsorption capacities were present in samples activated with ZnCl₂ reaching a maximum value at 178 V/V for sample MPZ7; it was prepared at 800 °C and 180 min of activation. The isotherms of Fig. 4a have the following order with respect to methane adsorption capacity: MPZ3 > MPP6 > MPK15 > MPC11. The values found in this research have the same order of magnitude of others reported in the literature and even in some activated carbons have higher values.

A similar behavior presents the CH₄ adsorption isotherms at different AA/char ratios = 2.0, 1.0 and 0.5 (see Fig. 4b–d). As seen in these figures, the adsorption behavior is the same as that of Fig. 4a for the ZnCl₂-activated samples. Table 4 shows the values of methane adsorption capacities for each sample.

The CH₄ adsorption results obtained for the samples prepared under the conditions reported here depend fundamentally on the microporosity developed in each of the samples, as several authors in the scientific literature have reported.

Table 4 Methane capacities of activated carbons prepared from mangosteen peel

Sample	Adsorption capacity at 25 °C and 3.5 MPa	
	$Q/\text{mmol g}^{-1}$	$VV^{-1}/\text{cm}^3 \text{ cm}^3$
MPP1	9.4	165.4
MPP2	10.7	167.1
MPP3	11.5	168.2
MPP4	12.7	169.3
MPZ5	9.9	173.4
MPZ6	10.11	175.3
MPZ7	11.23	177.3
MPZ8	11.78	178.1
MPC9	8.4	145.3
MPC10	8.78	148.3
MPC11	9.87	149.4
MPC12	10.34	150.5
MPK13	9.0	154.3
MPK14	9.89	155.1
MPK15	10.12	157.3
MPK16	10.90	159.8
MPP17	13.5	174.4
MPP18	14.5	175.5
MPZ19	15.7	178.4
MPZ20	16.3	179.3
MPC21	10.2	150.4
MPC22	11.3	154.2
MPK23	11.7	158.9
MPK24	12.6	160.3

By analyzing the results of the methane adsorption isotherms on the samples at a constant ratio (1.5) as well as the time (180 min) by different temperature (not shown in this publication), the result again is that the samples of activated carbons prepared with ZnCl₂ have the highest methane adsorption capacities. Values of 160 V/V were reached, suggesting that MP waste may be a suitable material to prepare activated carbons with a good performance for the storage of CH₄. In Table 5, there are some CH₄ adsorption capacities of other porous solids reviewed by the authors and Li et al. [14].

Methane differential enthalpy measurement by adsorption calorimetry: analysis

Figure 5 shows typical thermograms corresponding to the thermometric signal when injections of CH₄ are made on the activated carbons prepared in this investigation. The microcalorimeter senses heat conduction immediately after every injection of CH₄. This results in a peak of the exothermic process. The thermogram shows the potentiometric signal (recorded by thermopiles) as a function of time and equilibrium pressure.

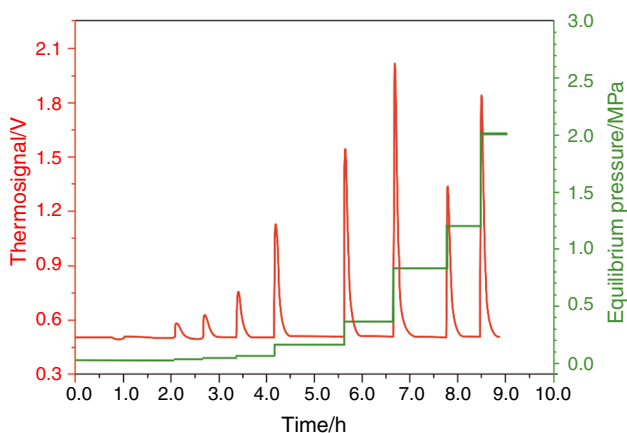
The CH₄ adsorption measures taken for this study were obtained by using the usual pressure and temperature reported in the literature (3.5 MPa and at 25 °C) to obtain comparable data. In thermodynamics, the differential enthalpy curves obtained by adsorption microcalorimetry allow the analysis both the adsorbate–adsorbent and the adsorbate–adsorbate interactions. From the analysis of the enthalpy curves, it is possible to study the mechanism of adsorbate filling and phase transitions, as well as any structural changes of the adsorbent.

Furthermore, it is also possible according to the form of the enthalpy-curves to establish and associate the differential enthalpies of adsorption with properties such as energetic heterogeneity and homogeneity of the surface, formation of the monolayer as well as relate with the presence of Lewis acid sites. In the particular case of this investigation, the interpretation of the entalpigrams was made fundamentally as a function of the energies developed during each CH₄ injection on the activated carbon, and it was associated with the homogeneity or heterogeneity of the surface.

For each prepared sample, the DRIFT-IR spectra were determined with the objective of analyzing the effect of each activating agent (publication in preparation). For example, for the case of MP activated with K₂CO₃ the IR bands established were: 3440–3253, 2374, 2355, 1999, 1654, 1437, 1288 and 1065 cm⁻¹, corresponding to the N–H, C≡C (alkynes), –COOH, C≡N, in-plane O–H (hydroxyl), –CH₂ (alkyl), C–O–C (ester, ether and phenol), C–O (anhydrides), out-plane O–H and out-plane C-derivates,

Table 5 Methane adsorption capacities compared with literature data

Sample	Brief description	$VV^{-1}/\text{cm}^3 \text{cm}^3$	Reference
MPZ20	AC from MP activated with ZnCl_2 (ratio: 1.5) at 900 °C	179.3	This work
Sample 6	AC from corn cob activated with KOH (ratio: 1) at 550 °C	120	[1]
AC- HNO_3	AC post-treated for HNO_3 solution (2 M) by 24 h at 110 °C	120.3	[2]
SMA-22	Monoliths from isotropic pitch-derived carbon and a powdered phenolic resin and CO_2 activation	150	[5]
LFC73	Carbon fiber activated with CO_2 with 73% of burn-off degree	163	[6]
CNS/2a	AC from coconut shell two-stage activation	143	[7]
DUT-6	MOF obtained from nickel and 1,3,5-tris(4-carboxyphenyl)benzene	126	[10]
PCN-14	MOF, PCN-14, based on a predesigned anthracene derivative, 5,5'-(9,10-anthracenediyl)-di-isophthalate	223	[12]
LMA-738	AC from olive stone activated with KOH (ratio: 5)	220	[14]
COF-102	Covalent organic framework is comprised of 3D structures with 3D medium-sized pores (12 Å)	145	[14]
PPN-4	Highly stable porous polymer networks	135	[14]
HKUST-1	MOF $\text{Cu}_3(\text{btc})_2$	267	[14]

**Fig. 5** Thermometric signal corresponding to the CH_4 adsorption on a sample of activated carbon (MPZ7)

while DRIFT-IR spectrum of MP activated with KOH evidences a marked influence that could be a result of the carbonization and activation process. Their characteristic bands between 1770 and 910 cm^{-1} corresponding to aromatic $\text{C}=\text{C}$ bands and oxygen functional groups were also present. The bands at 2940 cm^{-1} might be assigned to the active centers in potassium carbonates. This indicates that traces of the activating agent may be still present in the carbon matrix even after intensive washings [71]. Carbonyl groups $\text{C}=\text{O}$ and olefinic bonds $\text{C}=\text{C}$ are still present in the range $1745\text{--}1465 \text{ cm}^{-1}$, with lower intensity.

The DRIFT-IR spectrum corresponding to the MP activated with H_3PO_4 showed bands at $3350\text{--}3200 \text{ cm}^{-1}$ representing stretching vibration of $\text{O}\text{--}\text{H}$ in hydroxyl groups. The presence of this group in raw MP and AC was

reported in the literature [72, 73]. When comparing the DRIFT-IR spectrum of the AC with that of the starting material, it was observed that there is a removal of peaks at 2907 , 1737 , 1423 and 1325 cm^{-1} , which indicates the decomposition of functional groups present in oxygenated hydrocarbons. The intensity reduction in the band 1235 cm^{-1} in raw MP to 1218 cm^{-1} in MPP was due to the alteration of lignin structure containing the ester and ether linkage after the chemical treatment [74]. The band at 1737 cm^{-1} which corresponds to $\text{C}=\text{O}$ stretch in aldehydes, saturated aliphatic which present only in raw MP is due to thermal instability of aldehyde and ketone groups at high temperature [75]. However, introduction of peaks at 766 cm^{-1} showed the formation of bending vibration from: --C (triple bond), $\text{C}\text{--}\text{H}$ from alkynes and out-of-plane bending in benzene derivatives.

The DRIFT-IR spectrum of the MP impregnated with ZnCl_2 (MPZ) was carried out for both the starting material and the impregnated sample. Spectrum of the starting material shows many peaks belonging to different functional groups. The wide peak, which appears between 1000 and 1150 cm^{-1} , is related to ash composition, and side peaks at 1109 and $1160\text{--}1260 \text{ cm}^{-1}$ belong to alcoholic and phenolic groups. There is a peak at 1390 cm^{-1} that is not only related to carboxylate groups, but also it could be correlated with aliphatic alkanes depending on arrangement of organic structure in activation process. Existence of the peaks at 2930 and 2950 cm^{-1} supports this idea. The peak at 1630 and 3002 cm^{-1} belongs to aromatic $\text{C}=\text{C}$ and $\text{C}\text{--}\text{H}$ bonds, respectively, and they show the existence of aromatic character in raw material. The wide peak located

between 3100 and 3600 cm^{-1} belongs to phenolic OH groups, and the intensity of this peak decreases with formation of MPP (AC). This is another evidence of functionality loss in AC samples. The peaks located between 900 and 1200 cm^{-1} represent the ash content in the structure, and the ash content of the AC samples is very low. This shows that these peaks could belong to phenolic and alcoholic OH groups besides ash.

The DRIFT-IR spectrum of samples activated with K_2CO_3 (MPC) shows some bands associated with: surface functionalities with C=O (carboxylic, anhydride, lactone, and ketene groups having IR bands at 1750–1630 cm^{-1}), C–O (lactonic, ether, phenol, etc., with a very intensive band at 1300–1000 cm^{-1}) and C=C (1640–1430 cm^{-1}). In addition, weak bands at 2649 and 1154 cm^{-1} in MPC might be ascribed to the traces of potassium carbonates active centers beside metallic potassium that could be produced [76, 77]. This indicated that in spite of the extremely prolonged washing, a trace amount of potassium remained chemically bound inside the pore structure. An intensive band at 3700–3200 cm^{-1} of adsorbed water, which was observed, could mask a band of OH in different groups of CO–H. The results obtained by the DRIFT-IR study and enthalpigrams generate a good characterization of the thermodynamic phenomenon that occurs on the surface at the solid–vapor interface. This is possible because when a solid–vapor system is analyzed by adsorption microcalorimetry, an increase in the amount of adsorbed gas on the sample leads to an increase in the interactions between the adsorbate molecules. Also with respect to adsorbate–adsorbent contributions, the interaction of an adsorbate molecule with an energetically homogeneous surface shows a constant signal.

Finally, if the adsorbent is energetically heterogeneous due to a pore size distribution and/or a surface chemistry nature (defects, cations) a relatively strong interaction between the adsorbent molecules and the surface is expected. The strength of these interactions decreases as these specific sites are occupied. Thus, for the energetically heterogeneous adsorbents, a gradual decrease in the calorimetric signal is observed. However, each curve of differential enthalpy varies from one sample to another, showing an enthalpic contribution according to the textural characteristics of each activated carbon.

Figure 6a–d shows the differential adsorption enthalpies of CH_4 on each of the samples prepared from MP under the experimental conditions of this investigation.

Figure 6a shows the calorimetric isotherms corresponding to the differential enthalpy of CH_4 adsorption on the MPZ5 to MPZ8. The curves have the same tendency, and the three characteristic zones can be identified. The sample MPZ7 has the highest differential enthalpy not only of the samples presented in Fig. 6a but also compared with

the solids prepared with the other activating chemical agents: H_3PO_4 , K_2CO_3 and KOH.

The differential enthalpy of MPZ7 decreases (from about 115 to 63 kJ mol^{-1} for an adsorbed amount of 4.5 mmol g^{-1} of CH_4). This behavior is associated with the energetic heterogeneity of the surface as well as with a possible catalytic action between zinc and methane adsorbed on the surface of the activated carbon. As shown in Fig. 5a, all samples activated with ZnCl_2 have a similar behavior. It is interesting to note that the differential enthalpy generated during CH_4 adsorption under the experimental conditions described in this research varies as follows: MPZ7 > MPZ8 > MPZ6 > MPZ5. This result is associated with the characteristics developed by the MPZ samples when activated with ZnCl_2 in both their textural and chemical properties.

According to textural analysis, the activated carbons prepared with ZnCl_2 present not only the higher S_{BET} , but also this activating agent produced the highest micropore volume and the smaller diameter of micropores (see Fig. 3b), which is directly related to the higher values differential enthalpies of CH_4 adsorption. Therefore, this region (zone I) can be attributed to the amount adsorbed on the acid centers generated during the chemical activation with ZnCl_2 and the possible traces of the metal (Zn) and the CH_4 .

Then, a plate for the MPZ7 sample is presented which corresponds to the filling of the volume of micropores that were still empty. Zone II corresponds to the area of the surface that is energetically homogeneous once the heterogeneous sites of surface adsorption are occupied. In this sample, the plateau presents about 63 kJ mol^{-1} for 4.7–11.5 mmol g^{-1} .

An interesting behavior occurs in zone III where the differential enthalpies increase slightly. This behavior is associated with the possible interaction between the adsorbed CH_4 molecules. This means that the molecules that are inside the porous system and in particular those that have entered the microporous interact with van der Waals forces generating the slight increase in the enthalpies.

When analyzing the other curves (see Fig. 6b–d) for the MPP, MPC and MPK samples, respectively, they exhibit the same behavior. It changes the order of magnitude corresponding to the differential enthalpies of CH_4 adsorption. This is associated with the reactions generated during the chemical activation process because the use of these activating agents generates not only materials with good microporosity but also leaves traces of species interacting with the adsorbent that generate additional thermal effects. In the case of H_3PO_4 , for example, it can generate pyrophosphoric acid and polymetaphosphate among others, which may eventually lead to the formation

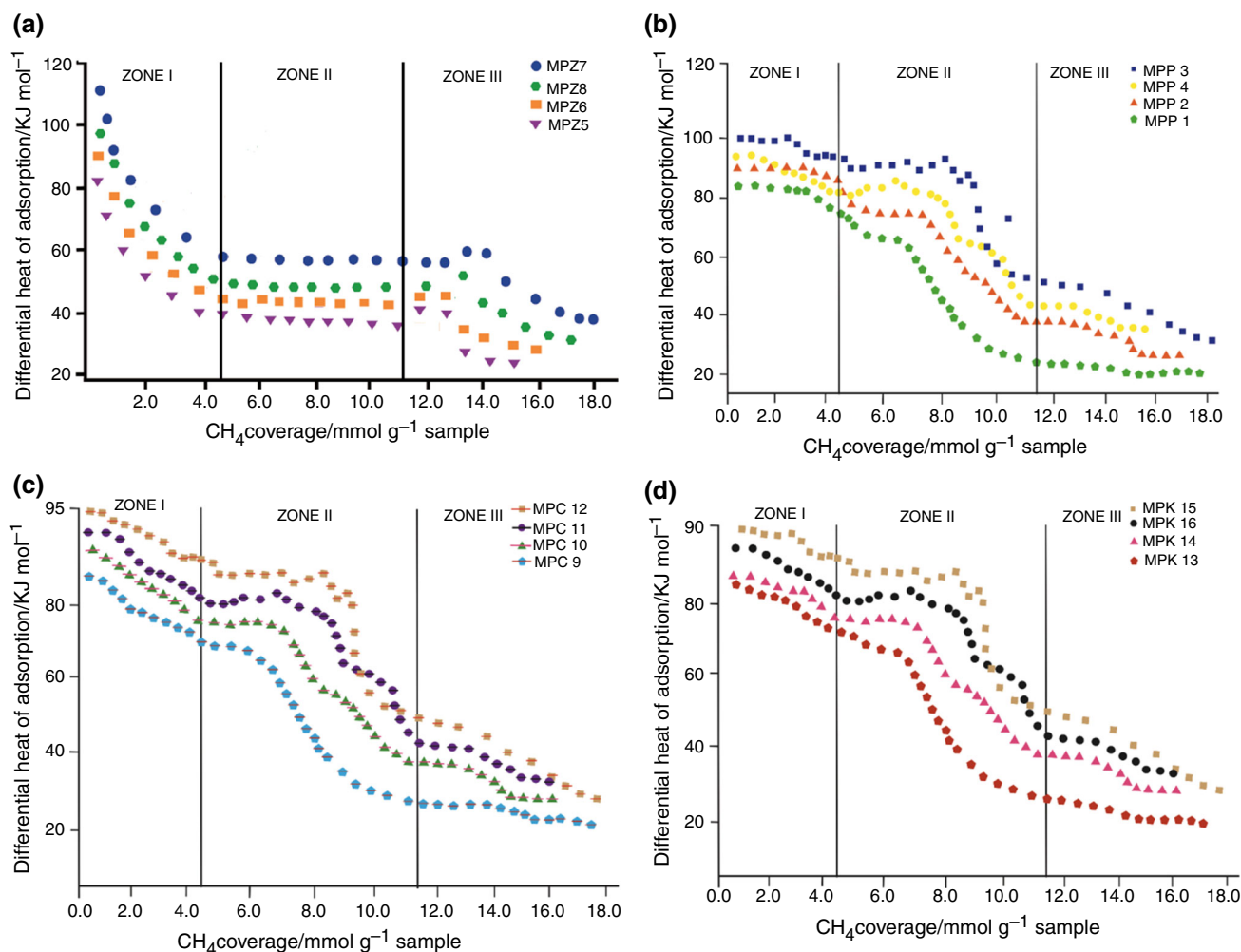


Fig. 6 Differential enthalpies of adsorption of CH_4 on the samples prepared from MP. **a** MPZ, **b** MPP, **c** MPC, **d** MPK

of C–O–P bonds, which allows for interactions between these atoms and CH_4 in addition to the heterogeneity of the carbonaceous surface [59, 78–82]. In the case of K_2CO_3 and KOH, they may also leave traces of the K metal during the chemical activation process [57, 58].

In summary, the CH_4 adsorption on the activated carbons prepared in this work presents a high differential enthalpy, which is associated with the development of a high microporosity generated during the carbons preparation, surface heterogeneity and traces left by the activating agents. In contrast to zone I, the differential enthalpy in zone II presents a plateau for all prepared samples corresponding to energetically homogeneous sites to finally reach zone III where the monolayer is reached.

Finally, it is noteworthy that in all the enthalpy-curves the zone I finishes at coverings around 5 mmol g^{-1} . This shows that a filling occurs on the smaller pores and in this investigation is around $0.5\text{--}1.0 \text{ nm}$. The results indicated that the adsorption microcalorimetry alone or in

combination with other techniques is a useful technique to characterize porous solids.

Conclusions

In this work, activated carbons were prepared from mangosteen peel (MP) by chemical activation using ZnCl_2 , H_3PO_4 , K_2CO_3 and KOH solutions as the activating agents to study the adsorption capacity of CH_4 . The samples presented BET surface areas from 915 to $1790 \text{ m}^2 \text{ g}^{-1}$ (MPC12 and MPZ20), whereas those activated with ZnCl_2 developed a larger volume of micropores. Methane storage was investigated by adsorption isotherms at high pressure and adsorption microcalorimetry measurements, and their results were compared.

A systematic study between the AA/char ratio and temperature was carried out, finding that at AA/char ratio of 1.5 and at a temperature of $800 \text{ }^\circ\text{C}$, samples with good textural characteristics were obtained. The methane storage

capacity was between 145 V/V (MPC9) and 180 V/V (MPZ20).

The results obtained by the adsorption microcalorimetry are in good agreement as mentioned above. The differential enthalpies of adsorption were determined for each of the samples by the application of CH₄ injections, obtaining well-defined thermograms allowing calculating the different areas under the curve of each peak due to the adsorption of CH₄ on the activated carbon. Finally, the results obtained by adsorption microcalorimetry allow associating the differential heats with the characteristics of the carbons.

Acknowledgements The authors wish to thank the framework agreement established between the Universidad Nacional de Colombia and Universidad de Los Andes (Bogotá, Colombia). Also they want to express their acknowledgments to the multinational EraNet-LAC project (ELAC2014/BEE-0367, BioFESS, Universität Hohenheim, Germany, project leader) and COLCIENCIAS Contract No. 217-2016 (Colombia) for the financial support to carry out this research.

References

1. Bagheri N, Abedi J. Adsorption of methane on corn cobs based activated carbon. *Chem Eng J*. 2011;89:2038–43.
2. Dai X, Liu X, Zhao G, Qian L, Qiao K, Yan Z. Treatment of activated carbon for methane storage. *Asia Pac J Chem Eng*. 2008;3:292–7.
3. El-Hendawy A, Samra S, Girgis B. Adsorption characteristics of activated carbons obtained from corncobs. *Colloids Surf A*. 2001;180:209–21.
4. Dai X, Liu X, Qian L, Yan Z, Zhang J. A novel method to synthesize super-activated carbon for natural gas adsorptive storage. *J Porous Mater*. 2006;13:399–405.
5. Burchell T, Rogers M. Low pressure storage of natural gas for vehicular applications 2000-01-2205. SAE Technical, 2000. <https://doi.org/10.4271/2000-01-2205>.
6. Lozano-Castello D, Alcaniz-Monge J, de la Casa-Lillo M, Cazorla-Amoros D, Linares-Solano A. Advances in the study of methane storage in porous carbonaceous materials. *Fuel*. 2002;81:1777–803.
7. Quinn D, Ragan S. Carbons suitable for medium pressure (6.9 MPa) methane storage. *Adsorpt Sci Technol*. 2000;18:515–27.
8. Biloe S, Goetz V, Mauran S. Characterization of adsorbent composite block for methane storage. *Carbon*. 2001;39:1653–62.
9. Lozano-Castello D, Lillo-Rodenas M, Cazorla-Amoros D, Linares-Solano A. Preparation of activated carbons from Spanish anthracite. I. Activation by KOH. *Carbon*. 2000;39:741–9.
10. Gedrich K, Senkovska I, Klein N, Stoeck U, Henschel A, Lohé MR, Baburin I, Mueller U, Kaskel S. A highly porous metal–organic framework with open nickel sites. *Angew Chem Int Ed*. 2010;49:8489–92.
11. Seki K. Design of an adsorbent with an ideal pore structure for methane adsorption using metal complexes. *Chem Commun*. 2001;16:1496–7.
12. Ma S, Sun D, Simmons J, Collier C, Yuan D, Zhou H. Metal–organic framework from an anthracene derivative containing nanoscopic cages exhibiting high methane uptake. *J Am Chem Soc*. 2008;130:1012–6.
13. Ma S, Zhou H. Gas storage in porous metal–organic frameworks for clean energy applications. *Chem Commun*. 2010;46:44–53.
14. Li B, Wen H, Zhou W, Xu J, Chen B. Porous metal–organic frameworks: promising materials for methane storage. *Chem*. 2016;1:557–80.
15. Beckner M, Dailly AA. A pilot study of activated carbon and metal–organic frameworks for methane storage. *Appl Energy*. 2016;162:506–14.
16. Wang H, Zhu Q, Zou R, Xu Q. Metal–organic frameworks for energy applications. *Chem*. 2017;2:52–80.
17. Ahmad M, Alrozi R. Optimization of preparation conditions for mangosteen peel-based activated carbons for the removal of Remazol Brilliant Blue R using response surface methodology. *Chem Eng J*. 2010;165:883–90.
18. Okonogi S, Duangrat C, Anuchpreeda S, Tachakittirungrod S, Chowwanapoonpohn S. Comparison of antioxidant capacities and cytotoxicities of certain fruit peels. *Food Chem*. 2007;103:839–46.
19. Zien R, Suhaili R, Earnestly F, Munaf E. Removal of Pb(II), Cd(II) and Co(II) from aqueous solution using *Garcinia mangostana* L. fruit shell. *J Hazard Mater*. 2010;181:52–6.
20. Chen Y, Huang B, Huang M, Cai B. On the preparation and characterization of activated carbon from mangosteen shell. *J Taiwan Inst Chem Eng*. 2011;42:837–42.
21. ASTM. ASTM D 3172 standard practice for proximate analysis of coal and coke. Philadelphia, PA: ASTM; 2012.
22. Moreno-Piraján JC, Giraldo L. Activated carbon obtained by pyrolysis of potato peel for the removal of heavy metal copper(II) from aqueous solution. *J Anal Appl Pyrolysis*. 2011;90:42–7.
23. Moreno-Piraján JC, Bastidas-Barranco MJ, Giraldo L. Preparation of activated carbons for storage of methane and its study by adsorption calorimetry. *J Therm Anal Calorim*. 2017. <https://doi.org/10.1007/s10973-017-6132-8>.
24. Correia LB, Fiuza RA, Andrade RC, Andrade H. CO₂ capture on activated carbons derived from mango fruit (*Mangifera indica* L.) seed shells: a TG study. *J Therm Anal Calorim*. 2017. <https://doi.org/10.1007/s10973-017-6542-7>.
25. Wu M, Shi L, Mi J. Preparation and desulfurization kinetics of activated carbons from semi-coke of coal liquefaction residual. *J Therm Anal Calorim*. 2017;129:1593–603.
26. ASTM. ASTM D 4607-94, standard test method for determination of iodine number of activated carbon. Philadelphia, PA: ASTM; 2006.
27. Elliott C, Colby TV, Kelly TM, Hicks HG. Charcoal lung: bronchiolitis obliterans after aspiration of activated charcoal. *Chest*. 1989;96:672–4.
28. Ceyhan A, Sahin Ö, Baytar O, Saka C. Surface and porous characterization of activated carbon prepared from pyrolysis of biomass by two-stage procedure at low activation temperature and its adsorption of iodine. *J Anal Appl Pyrolysis*. 2013;104:378–83.
29. Cychosz K, Guo X, Fan W, Cimino R, Gor G, Tsapatsis M, Neimark A, Thommes M. Characterization of the pore structure of three-dimensionally ordered mesoporous carbons using high resolution gas sorption. *Langmuir*. 2012;28:12647–54.
30. Neimark A, Lin Y, Ravikovitch P, Thommes M. Quenched solid density functional theory and pore size analysis of micro-mesoporous carbons. *Carbon*. 2009;47:1617–28.
31. Rodríguez-Reinoso F, Garrido J, Martín-Martínez J, Molina Sabio M, Torregrosa R. The combined use of different approaches in the characterization of microporous carbons. *Carbon*. 1989;27:23–32.
32. Roquerol J, Llewellyn P, Rouquerol F. Is BET equation applicable to microporous adsorbents? In: Lewelling P, Rodriguez Reinoso F, Rouquerol J, Seaton N, editors. Characterization of

- porous solids VII. Studies in surface science and catalysis. Amsterdam: Elsevier; 2007. p. 49–56.
33. Thommes M, Cychosz KA. Characterization of nanoporous materials: progress and challenges. *Adsorption*. 2014;20:233–50.
 34. Brunauer S, Emmett P, Teller E. Adsorption of gases in multimolecular layers. *J Am Chem Soc*. 1936;40:7:309–13.
 35. Lippens B, de Boer J. Studies on pore systems in catalysts: V. The t-method. *J Catal*. 1965;4:319–23.
 36. Luo J, Liu Y, Jian C, Chu W, Jie W, Xie H. Experimental and modeling study of methane adsorption on activated carbon derived from anthracite. *J Chem Eng Data*. 2011;56:4919–26.
 37. Luo J, Liu Y, Sun W, Jiang C, Xie H, Chu W. Influence of structural parameters on methane adsorption over activated carbon: evaluation by using D–A model. *Fuel*. 2014;123:241–7.
 38. Giraldo L, Bastidas-Barranco M, Moreno-Piraján JC. Adsorption calorimetry: energetic characterisation of the surface of mesoporous silicas and their adsorption capacity of non-linear chain alcohols. *Colloids Surf A*. 2016;496:100–13.
 39. Garcia-Cuello V, Moreno-Piraján J, Giraldo-Gutiérrez L, Sapag K, Zgrablich G. A new microcalorimeter of adsorption for the determination of differential enthalpies. *Microporous Mesoporous Mater*. 2009;120:239–45.
 40. Ahmadpour A, Do D. The preparation of activated carbon from macadamia nutshell by chemical activation. *Carbon*. 1997;35:1723–32.
 41. Tran T, Bui Q, Nguyen T. A comparative study on the removal efficiency of metal ions (Cu^{2+} , Ni^{2+} , and Pb^{2+}) using sugarcane bagasse-derived ZnCl_2 -activated carbon by the response surface methodology. *Adsorpt Sci Technol*. 2016;25:72–85.
 42. Girgis B, Ishak M. Activated carbon from cotton stalks by impregnation with phosphoric acid. *Mater Lett*. 1999;39:107–14.
 43. Caturla F, Molina-Sabio M, Rodriguez-Reinoso F. Preparation of activated carbon by chemical activation with ZnCl_2 . *Carbon*. 1991;29:999–1007.
 44. Adinata D, Daud W, Aroua M. Preparation and characterization of activated carbon from palm shell by chemical activation with K_2CO_3 . *Bioresour Technol*. 2007;98:145–9.
 45. Li W, Peng J, Zhang L, Xia H, Li N, Yang K, Zhu X. Effects of characterization temperatures on characteristics of porosity in coconut shell chars and activated carbons derived from carbonized coconut shell chars. *J Ind Crops Prod*. 2008;28:73–8.
 46. Devi A, Latif P, Tham Y, Taufiq-Ya Y. Physical characterization of activated carbon derived from mangosteen peel. *Asian J Chem*. 2012;24:579–83.
 47. Kalderis D, Bethanis S, Paraskeva P, Diamadopoulos E. Production of activated carbon from bagasse and rice husk by a single-stage chemical activation method at low retention times. *Bioresour Technol*. 2008;99:6809–16.
 48. Williams P, Besler S. The pyrolysis of rice husks in a thermogravimetric analyzer and static batch reactor. *Fuel*. 1993;72:151–9.
 49. Özsın G, Pütün AE. Kinetics and evolved gas analysis for pyrolysis of food processing wastes using TGA/MS/FT-IR. *Waste Manag*. 2017;64:315–26.
 50. Meng A, Chen S, Long Y, Zhou H, Zhang Y, Li Q. Pyrolysis and gasification of typical components in wastes with macro-TGA. *Waste Manag*. 2015;46:247–56.
 51. Mundike J, Collard F, Görgens J. Pyrolysis of *Lantana camara* and *Mimosa pigra*: influences of temperature, other process parameters and incondensable gas evolution on char yield and higher heating value. *Bioresour Technol*. 2017;243:284–93.
 52. Collard F, Blin J. A review on pyrolysis of biomass constituents: mechanisms and composition of the products obtained from the conversion of cellulose, hemicelluloses and lignin. *Renew Sustain Energy Rev*. 2014;38:594–608.
 53. Zabaniotou A, Ioannidou O, Antonakou E, Lappas A. Experimental study of pyrolysis for potential energy, hydrogen and carbon material production from lignocellulosic biomass. *Int J Hydrog Energy*. 2008;33:2433–44.
 54. Meng A, Zhang Y, Zhuo J, Li Q, Qin L. Investigation on pyrolysis and carbonization of *Eupatorium adenophorum* Spreng and tobacco stem. *J Energy Inst*. 2015;88:480–9.
 55. White JE, Catallo WJ, Legendre BL. Biomass pyrolysis kinetics: a comparative critical review with relevant agricultural residue case studies. *J Anal Appl Pyrol*. 2011;91:1–33.
 56. Thommes M, Kaneko K, Neimark A, Olivier J, Rodriguez-Reinoso F, Rouquerol J, Sing K. Physisorption of gases, with special reference to the evaluation of surface area and pore size distribution (IUPAC Technical Report). *Pure Appl Chem*. 2015;87:1051–69.
 57. Van K, Thi T. Activated carbon derived from rice husk by NaOH activation and its application in supercapacitor. *Prog Nat Sci Mater*. 2014;24:191–8.
 58. Cao Q, Xie K, Lv Y, Bao W. Process effects on activated carbon with large specific surface area from corn cob. *Bioresour Technol*. 2006;97:110–5.
 59. Kan Y, Yue Q, Li D, Wu Y, Gao B. Preparation and characterization of activated carbons from waste tea by H_3PO_4 activation in different atmospheres for oxytetracycline removal. *J Taiwan Inst Chem Eng*. 2017;71:494–500.
 60. Landers J, Gor G, Neimark A. Density functional theory methods for characterization of porous materials. *Colloids Surf A Physicochem Eng Asp*. 2013;437:3–32.
 61. Gor G, Thommes M, Cychosz K, Neimark A. Quenched solid density functional theory method for characterization of mesoporous carbons by nitrogen adsorption. *Carbon*. 2012;50:1583–90.
 62. Jimenez-Cordero D, Heras F, Alonso-Morales N, Gilarranz MA, Rodriguez JJ. Development of porosity upon physical activation of grape seeds char by gas phase oxygen chemisorption–desorption cycles. *Chem Eng J*. 2013;231:172–81.
 63. Jimenez-Cordero D, Heras F, Alonso-Morales N, Gilarranz MA, Rodriguez JJ. Porous structure and morphology of granular chars from flash and conventional pyrolysis of grape seeds. *Biomass Bioenergy*. 2013;54:123–32.
 64. Kilic M, Apaydin-Varol E, Putun AE. Preparation and surface characterization of activated carbons from *Euphorbia rigida* by chemical activation with ZnCl_2 , K_2CO_3 , NaOH and H_3PO_4 . *Appl Surf Sci*. 2012;261:247–54.
 65. Zhu G, Deng X, Hou M, Sun K, Zhang Y, Li P, Liang F. Comparative study on characterization and adsorption properties of activated carbons by phosphoric acid activation from corncob and its acid and alkaline hydrolysis residues. *Fuel Process Technol*. 2016;144:255–61.
 66. Shamsuddin MS, Yusoff N, Sulaiman MA. Synthesis and characterization of activated carbon produced from kenaf core fiber using H_3PO_4 activation. *Procedia Chem*. 2016;19:558–65.
 67. Tay T, Ucar S, Karagoz S. Preparation and characterization of activated carbon from waste biomass. *J Hazard Mater*. 2009;165:481–5.
 68. Ji Y, Li T, Zhu L, Wang X, Lin Q. Preparation of activated carbons by microwave heating KOH activation. *Appl Surf Sci*. 2007;254:506–12.
 69. Byamba-Ochir N, Shim W, Balathanigaimani MS, Moon H. High density Mongolian anthracite based porous carbon monoliths for methane storage by adsorption. *Appl Energy*. 2017;190:257–65.
 70. Loh W, Rahman K, Chakraborty A, Saha BB, Choo YS, Khoo Ch, Choon K. Improved isotherm data for adsorption of methane on activated carbons. *Chem Eng Data*. 2010;55:2840–7.

71. El-Hendawy AN. An insight into the KOH activation mechanism through the production of microporous activated carbon for the removal of Pb^{2+} cations. *Appl Surf Sci.* 2009;255:3723–30.
72. Chowdhury ZZ, Zain SM, Khan RA, Islam S. Preparation and characterizations of activated carbon from kenaf fiber for equilibrium adsorption studies of copper from wastewater. *J Appl Sci Eng Technol.* 2012;29:1187–95.
73. Jonoobi M, Harun J, Shakeri A, Misra M, Oksmand K. Chemical composition, crystallinity and thermal degradation of bleached and unbleached kenaf bast (*Hibiscus cannabinus*) pulp and nanofibers. *BioResources.* 2009;4:626–39.
74. Khadiran T, Hussein MZ, Zainal Z, Rusli R. Textural and chemical properties of activated carbon prepared from tropical peat soil by chemical activation method. *BioResources.* 2015;10:986–1007.
75. Hamza UD, Nasri NS, Amin NS, Mohammed J, Zain HM. Characteristics of oil palm shell biochar and activated carbon prepared at different carbonization times. *Desalin Water Treat.* 2015;5:1–8.
76. Gomez-Serrano V, Pastor-Viilegas J, Perez-Florin A, Duran-Valle C, Valenzuela-Calahorra C. FT-IR study of rockrose and of char and activated carbon. *J Anal Appl Pyrolysis.* 1996;36:71–80.
77. El-Hendawy AA. Variation in the FTIR spectra of a biomass under impregnation, carbonization and oxidation conditions. *J Anal Appl Pyrolysis.* 2006;75:159–66.
78. Suárez-García F, Martínez-Alonso A, Tascón J. Activated carbon fibers from Nomex by chemical activation with phosphoric acid. *Carbon.* 2004;42:1419–26.
79. Liu H, Wang X, Zhai G, Zhang J, Zhang C, Bao N, Cheng C. Preparation of activated carbon from lotus stalks with the mixture of phosphoric acid and pentaerythritol impregnation and its application for Ni(II) sorption. *Chem Eng J.* 2012;209:155–62.
80. Benaddi H, Legras D, Rouzaud JN, Beguin F. Influence of the atmosphere in the chemical activation of wood by phosphoric acid. *Carbon.* 1998;36:306–9.
81. Guo J, Lua A. Textural and chemical properties of adsorbent prepared from palm shell by phosphoric acid activation. *Mater Chem Phys.* 2003;80:114–9.
82. Girgis B, Yunis S, Soliman A. Characteristics of activated carbon from peanut hulls in relation to conditions of preparation. *Mater Lett.* 2002;57:164–72.